Inorganic Chemistry

Article

pubs.acs.org/IC

6-(Tetrazol-5-yl)-2,2′-bipyridine: A Highly Selective Ligand for the Separation of Lanthanides(III) and Actinides(III)

Jochen Kratsch,[†] Björn B. Beele,[‡,§] Carsten Koke,[‡] Melissa A. Denecke,[∥] Andreas Geist,[§] Petra J. Panak,*[,‡,§] and Peter W. Roesky*[,†]

[†]Institut für Anorganische Chemie, Karlsruher Institut für Technologie, Engesserstrasse 15, 76131 Karlsruhe, Germany

[‡]Physikalisch-Chemisches Institut, Ruprecht-Karls-Universität Heidelberg, Im Neuenheimer Feld 253, 69120 Heidelberg, Germany

[§]Institut für Nukleare Entsorgung, Karlsruher Institut für Technologie, P.O. Box 3640, 76021 Karlsruhe, Germany

[∥]Dalton Nuclear Institute, Pariser Building, Floor G, Sackville Street, and The University of Manchester, Manchester M13 9PL, United Kingdom

Supporting Information

ABSTRACT: The coordination structure in the solid state and solution complexation behavior of 6-(tetrazol-5-yl)-2,2′-bipyridine (HN_4bipy) with samarium(III) was investigated as a model system for actinide(III)/lanthanide(III) separations. Two different solid 1:2 complexes, $[Sm(N_4bipy)_2(OH)(H_2O)_2]$ (**1**) and $[Sm(N_4bipy)_2(HCOO)(H_2O)_2]$ (**2**), were obtained from the reaction of samarium(III) nitrate with HN_4bipy in isopropyl alcohol, resuspension in *N*,*N*-dimethylformamide (DMF), and slow crystallization. The formate anion coordinated to samarium in **2** is formed by decomposition of DMF to formic acid and dimethylamine. Time-resolved laser fluorescence spectroscopy (TRLFS) studies were performed with curium(III) and europium(III) by using HN_4bipy as the ligand. Curium(III) is observed to form 1:2 and 1:3 complexes with increasing HN_4bipy concentration; for europium(III), formation of 1:1 and 1:3 complexes is observed. Although the solid-state samarium complexes were confirmed as 1:2 species the 1:2 europium(III) solution complex in ethanol was not identified with TRLFS. The determined conditional stability constant for the 1:3 fully coordinated curium(III) complex species is more than 2 orders of magnitude higher than that for europium(III) (log $\beta_3[Cm(N_4bipy)_3]$ = 13.8 and log $\beta_3[Eu(N_4bipy)_3]$ = 11.1). The presence of added 2-bromodecanoic acid as a lipophilic anion source reduces the stability constant for formation of the 1:2 and 1:3 curium(III) complexes, but no ternary complexes were observed. The stability constants for the 1:3 metal ion−N_4bipy complexes equate to a theoretical separation factor, $SF_{Cm^{III}/Eu^{III}} \approx 500$. However, the low solubility of the HN_4bipy ligand in nonpolar solvents typically used in actinide−lanthanide liquid−liquid extractions prevents its use as a partitioning extractant until a more lipophilic HN_4bipy-type ligand is developed.

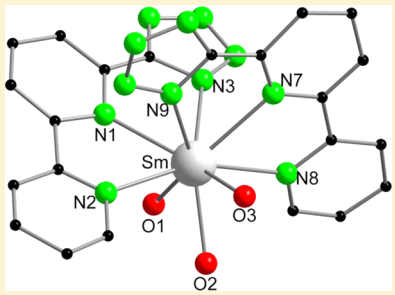

INTRODUCTION

As of 2010, about 13% of the world's electricity was supplied by nuclear power plants,[1] and in doing so, 10500 tons of used nuclear fuel accumulated annually.[2] One of the major challenges of the nuclear fuel cycle is the long-term radiotoxicity and thermal power of used nuclear fuel. The long-term radiotoxicity and thermal power are dominated by plutonium and the minor actinides (MA = Np, Am, and Cm) after a cooling period of approximately 100 years. Reducing the content of these in the waste before storage is the aim of the Partitioning and Transmutation strategy. The basic idea is to separate plutonium and the MAs with their long-lived, highly toxic isotopes from high-level radioactive waste (partitioning) and convert them by neutron fission (transmutation) into shorter-lived and stable isotopes. Because some of the lanthanides possess large neutron cross sections, it is necessary to separate them from the trivalent actinides to ensure sufficient transmutation efficiency. One of the most promising processes for the separation of trivalent MAs (Am^{III} and Cm^{III}) from the chemically similar lanthanide ions (Ln^{III}) is the use of solvent extraction, which requires suitable complexing agents. Whereas common oxygen-donor ligands do not show the desired selectivity, soft nitrogen- or sulfur-donor ligands exhibit higher affinities for the trivalent MAs over Ln^{III}.[3−10]

Thus, nitrogen heterocyclic compounds form stronger complexes with trivalent actinides than with lanthanides.[8] Unfortunately, most of these compounds do not work at low pH, which is a process requirement. The first nitrogen-donor extractants reported to selectively extract Am^{III} and Cm^{III} over Ln^{III} cations with separation factors for Am^{III} over Eu^{III} higher than 100 under acidic conditions were the alkylated 2,6-bis(1,2,4-triazin-3-yl)pyridines (BTPs; Scheme 1).[11,12] BTPs are known to form symmetric 1:3 complexes $[M(BTP)_3]^{3+}$ with both trivalent actinides and lanthanides,[8,13−19] and some ligands fulfill additional important requirements for a potent extractant like stability toward high radiation and acidity, fast extraction kinetics, and high solubility.[8] Although the complex-

Received: March 31, 2014
Published: June 26, 2014

   dx.doi.org/10.1021/ic5007549 | *Inorg. Chem.* 2014, 53, 8949−8958

Scheme 1. Molecular Structure of the Alkylated BTPs

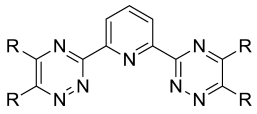

R = CH_3, C_2H_5, *n*-C_3H_7, *i*-C_3H_7, *n*-C_4H_9, *i*-C_4H_9

ation and extraction properties of many BTP-type ligands are well-examined, a comprehensive understanding of some ligands' selectivity is still missing on a molecular level. Consequently, advances in the extraction performance have in the past largely been based on empirical trial and error. However, systematic modifications were carried out on BTP-type ligands in order to optimize the complexation and extraction performance. This includes structural changes in the lateral rings[20−26] and alkylation of the substituents at the molecule periphery[8,27,28] or the substituents on the pyridine ring.[29]

In an effort to define the influence of the ligand geometry on the coordination behavior, we made minor modifications on the BTP ligand system. For this purpose, the coordination and extraction properties of the nitrogen-donor ligands 6-(3,5-dimethyl-1*H*-pyrazol-1-yl)-2,2′-bipyridine (dmpbipy),[23] 2,6-bis-[5-(2,2-dimethylpropyl)-1*H*-pyrazol-3-yl]pyridine (C5-BPP),[20,21] 2,6-bis(4-ethylpyridazin-1-yl)pyridine (Et-BDP),[24] and 2,6-bis(4-*n*-propyl-2,3,5,6-tetrazin-1-yl)pyridine (^{n}Pr-Tetrazine)[24] were examined in previous studies (see Scheme 2). As a

Scheme 2. Molecular Structures of HN_4bipy, dmpbipy,[23] C5-BPP,[13,14] Et-BDP,[16] and ^{n}Pr-Tetrazine.[16]

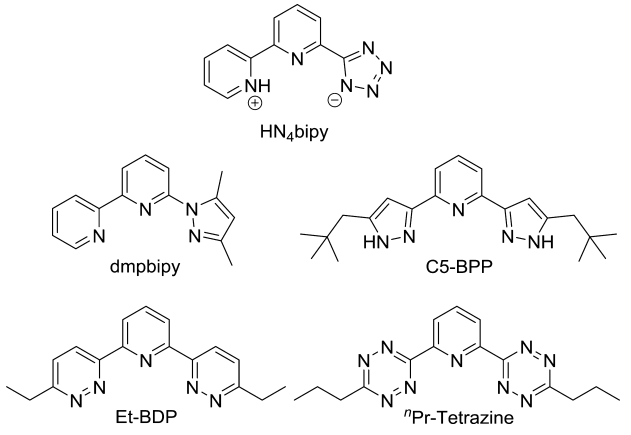

further modification of these systems, the complexing properties of 6-(tetrazol-5-yl)-2,2′-bipyridine (HN_4bipy) are reported here. It can be regarded as a nitrogen-rich variation of dmpbipy, in which the pyrazolyl ring is substituted by a tetrazolyl unit.

In the present work, the syntheses of HN_4bipy and its complexes with samarium(III) are described. Important thermodynamic data for the complex formation of HN_4bipy with curium(III), as well as europium(III), were determined by time-resolved laser fluorescence spectroscopy (TRLFS). Finally, the results for liquid−liquid extraction studies for americium(III) and europium(III) are discussed.

EXPERIMENTAL SECTION

Syntheses. 6-Cyano-2,2′-bipyridine[30] was prepared according to the literature procedure. Deuterated solvents were obtained from Aldrich (99 atom % D). NMR spectra were recorded on a Bruker Avance II 300 MHz spectrometer. Chemical shifts are referenced to internal solvent resonances and are reported relative to tetramethylsilane (^{1}H and ^{13}C NMR). IR spectra were obtained on a Bruker Tensor 37 FT IR spectrometer. Electrospray ionization mass spectrometry (ESI-MS) spectra were recorded on Bruker MicroTOF and IonSpec FT-ICR (7 T) ESI-MS spectrometers. Elemental analyses were carried out with a Vario MICRO cube.

HN_4bipy. The synthesis of HN_4bipy was performed according to the procedure reported by Chi et al.[31] from 6-cyano-2,2′-bipyridine,

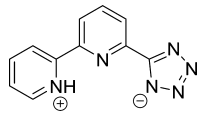

sodium azide, and ammonium chloride in *N*,*N*-dimethylformamide (DMF). Single crystals were obtained by crystallization from isopropyl alcohol. Yield: 65%. ^{1}H NMR (DMSO-d_6, 400 MHz, 25 °C): δ 8.86−8.79 (m, 2H, $H_{d,e}$), 8.59 (dd, $^3J_{H,H}$ = 7.40 Hz, $^4J_{H,H}$ = 1.55 Hz, 1H, H_a), 8.31−8.18 (m, 3H, H, $H_{c,f,g}$), 7.69−7.65 (m, 1H, H_b). ^{13}C{^{1}H} NMR (DMSO-d_6, 75 MHz, 25 °C): δ 155.0, 154.2, 152.8, 148.3, 143.7, 140.3, 140.1, 126.0, 123.5, 123.2, 122.6. The NMR data are in accordance with the literature.[31]

[$Sm(N_4bipy)_2(OH)(H_2O)_2$] (1) and [$Sm(N_4bipy)_2(HCOO)(H_2O)_2$] (2). [$Sm(NO_3)_3{\cdot}6H_2O$] (93 mg, 0.21 mmol) and HN_4bipy (141 mg, 0.63 mmol) were suspended in 10 mL of isopropyl alcohol and refluxed for 24 h. After cooling to room temperature, 90 mL of isopropyl alcohol were added to the suspension and stirred for additional 24 h. The resulting precipitate was filtered off and dissolved in DMF. Standing at room temperature for 2 weeks leads to colorless crystals of **1**. Yield: 30 mg, 46 μmol, 22%. ^{1}H NMR (DMSO-d_6, 300 MHz, 25 °C): δ 8.87−8.49 (br m, 4 H), 8.46−8.17 (br m, 2 H), 8.28−8.26 (br m, 2H), 8.07 (t, ^3J = 7.7 Hz, 2H), 7.99−7.57 (br m, 2H), 7.41 (br s, 2H). ^{13}C{^{1}H} NMR (DMSO-d_6, 75 MHz, 25 °C): δ 162.4, 154.7, 150.5, 149.5, 149.4, 141.2, 140.2, 124.4, 122.0, 121.4. In ^{13}C NMR, only 10 of the expected 11 carbon signals due to broadened bands were observed. IR (ATR): ν 3366 (m), 3218 (m), 3081 (w), 3060 (w), 3035 (w), 1662 (m), 1596 (m), 1572 (m), 1486 (w), 1463 (w), 1432 (m), 1420 (m), 1392 (w), 1376 (m), 1297 (w), 1268 (w), 1245 (w), 1187 (w) cm^{-1}. ESI-MS (DMF): *m*/*z* 689.12 ([$Sm(N_4bipy)_2(H_2O)(dmf)$]$^+$), 669.72 ([$Sm(N_4bipy)_2(OH)_2(H_2O)_2$]$^-$), 596.55 ([$Sm_2(N_4bipy)_4$]$^{2+}$) amu. Elem anal. Calcd for $C_{22}H_{19}N_{12}O_3Sm$ (**1**)·$4H_2O$ (721.89): C, 36.60; H, 3.77; N, 23.28. Found: C, 36.55; H, 3.88; N, 22.54.

After 12 weeks, colorless crystals of **2** were obtained from the mother liquor. Yield: 15 mg, 21 μmol, 10%. ^{1}H NMR (DMSO-d_6, 300 MHz, 25 °C): δ 8.68−8.44 (br, 4H, Py), 8.44−8.20 (br, 5H, Py and $HCOO^-$), 8.15−7.98 (br, 3H, Py), 7.48−7.27 (br, 3H, Py). A ^{13}C{^{1}H} NMR spectrum could not be obtained because of the poor solubility and the paramagnetism of the complex. IR (ATR): ν 3075 (w), 2925 (w), 1665 (m), 1586 (s), 1568 (s), 1519 (w), 1487 (w), 1462 (m), 1430 (m), 1391 (w), 1372 (m), 1243 (w), 1213 (w), 1182 (w), 1161 (w), 1149 (w), 1128 (w), 1110 (w), 1100 (w), 1060 (m), 1043 (w), 1010 (m), 838 (m), 810 (w), 788 (m), 765 (s), 740 (m), 690 (m), 668 (m), 650 (m), 631 (w), 595 (w), 542 (w), 521 (w), 502 (w) cm^{-1}. ESI-MS (DMF): *m*/*z* 822.13 ([$Sm(N_4bipy)_2(HN_4bipy)$]$^+$), 744.13 ([$Sm(N_4bipy)_2(dmf)_2$]$^+$) amu.

X-ray Crystallographic Studies of HN_4bipy, 1, and 2. A suitable crystal was covered in mineral oil (Aldrich) and mounted onto a glass fiber. The crystal was transferred directly to a N_2 cold stream of a Stoe IPDS 2 or a Stoe Stadivari diffractometer. All structures were solved by direct or Patterson methods (*SHELXS-97*).[32] The remaining non-hydrogen atoms were located from successive difference Fourier map calculations. The refinements were carried out by using full-matrix least-squares techniques on F^2, minimizing the function $(F_o - F_c)^2$, where the weight is defined as $4F_o^2/2F_o^2$ and F_o and F_c are the observed and calculated structure factor amplitudes using the program *SHELXL-97*.[32] The carbon-bound hydrogen-atom positions were calculated. The hydrogen-atom contributions were calculated but not refined. The locations of the largest peaks in the final difference

dx.doi.org/10.1021/ic5007549 | Inorg. Chem. 2014, 53, 8949−8958

Fourier map calculations, as well as the magnitude of the residual electron densities, in each case were of no chemical significance.

Crystal data for HN_4bipy: $C_{11}H_8N_6 \cdot 3H_2O$, M = 278.28, monoclinic, a = 8.812(2) Å, b = 21.639(4) Å, c = 7.1094(14) Å, β = 104.94(3)°, V = 1309.8(5) Å^3, T = 200(2) K, space group $P2_1/c$, Z = 4, μ = 0.107 mm^{-1}, 9290 reflections measured, 3500 independent reflections (R_{int} = 0.0915). The final R1 values were 0.0569 [$I > 2\sigma(I)$]. The final wR2(F^2) values were 0.0983 (all data). The goodness of fit on F^2 was 0.860.

Crystal data for **1**: $C_{22}H_{19}N_{12}O_3Sm \cdot 3.5H_2O$, M = 712.90, monoclinic, a = 11.052 Å, b = 11.334 Å, c = 12.725 Å, β = 106.18°, V = 1530.9 Å^3, T = 100(2) K, space group $P2/n$, Z = 2, μ = 1.975 mm^{-1}, 11005 reflections measured, 2863 independent reflections (R_{int} = 0.1524). The final R1 values were 0.0870 [$I > 2\sigma(I)$]. The final wR2(F^2) values were 0.2364 (all data). The goodness of fit on F^2 was 0.962.

Crystal data for **2**: $C_{23}H_{19}N_{12}O_4Sm \cdot 2DMF$, M = 824.04, triclinic, a = 11.681(2) Å, b = 12.438(3) Å, c = 12.515(3) Å, α = 73.41(3)°, β = 84.43(3)°, γ = 69.86(3)°, V = 1635.9(6) Å^3, T = 100(2) K, space group $P\bar{1}$, Z = 2, μ = 1.861 mm^{-1}, 27763 reflections measured, 5911 independent reflections (R_{int} = 0.0535). The final R1 values were 0.0209 [$I > 2\sigma(I)$]. The final wR2(F^2) values were 0.0532 (all data). The goodness of fit on F^2 was 1.106.

TRLFS Solution Preparation. A 10^{-2} mol L^{-1} HN_4bipy ligand stock solution is prepared by dissolving 11.2 mg (50.0 μmol) of HN_4bipy in 5.0 mL of ethanol (EtOH; 4.4 vol % H_2O). The stock solution is diluted to 10^{-3} mol L^{-1} and 10^{-4} mol L^{-1}, when needed. The water content is adjusted to 4.4 vol % H_2O. For titrations in the presence of the lipophilic anion source 2-bromodecanoic acid, 1.1 mg (5.0 μmol) of HN_4bipy is dissolved in a mixture of 0.104 mL (0.5 mmol) of 2-bromodecanoic acid and 4.896 mL of EtOH (4.4 vol % H_2O), resulting in a 10^{-3} mol L^{-1} ligand solution. 1.0×10^{-7} mol L^{-1} $Cm(ClO_4)_3$ sample solutions are prepared by adding 15 μL of an aqueous stock solution of $Cm(ClO_4)_3$ (6.7×10^{-6} mol L^{-1} in 0.01 mol L^{-1} $HClO_4$) to 29 μL of H_2O and 956 μL of EtOH or a mixture of 21 μL of 2-bromodecanoic acid (0.1 mmol), 29 μL of H_2O, and 935.2 μL of EtOH, respectively. For a 4.0×10^{-5} mol L^{-1} $Eu(ClO_4)_3$ sample solution, 44.4 μL of an aqueous $Eu(ClO_4)_3$ stock solution (9.0×10^{-4} mol L^{-1} in 0.01 mol L^{-1} $HClO_4$) is added to 955.6 μL of EtOH.

TRLFS Setup. TRLFS measurements are performed using a Nd:YAG-pumped dye laser system [Surelite II laser (Continuum), NARROWscan D-R dye laser (Radiant Dyes Laser Accessories)]. For Eu^{III} excitation, a wavelength of 394.0 nm was used, and for Cm^{III} excitation, a wavelength of 396.6 nm was used. The fluorescence emission is recorded at an angle of 90° to the exciting laser beam. A Shamrock 303i spectrograph (ANDOR), equipped with a 300, 900, and 1200 lines mm^{-1} grating turret, is used for spectral decomposition. The fluorescence emission is detected by an ICCD camera [iStar Gen III, A-DH 720 18F-63 (ANDOR)]. Rayleigh scattering and short-lived fluorescence of organic ligands are discriminated by a delay time of 1.0 μs before the fluorescence light is recorded. The gate width for all measurements was set to 1.0 ms. The quartz cuvette is temperature-controlled at T = 25 °C. Titrations are performed by the stepwise addition of a HN_4bipy solution in EtOH (4.4 vol % H_2O) or EtOH/0.1 mol L^{-1} 2-bromodecanoic acid, respectively, to a curium(III) or europium(III) solution in the same solvent. The solutions are allowed to equilibrate for 10 min before the fluorescence is recorded. For curium(III) and europium(III) lifetime measurements, the decay of the emission intensity is scanned with time steps of 20 and 50 μs, respectively. The fluorescence lifetime τ is obtained by fits of the fluorescence intensity I versus the delay time t after the laser pulse to the equation $I(\lambda) = I_0(\lambda) \exp(-\tau/t)$.

X-ray Absorption Near-Edge Structure (XANES) Studies. Sm L3-edge XANES measurements of the samarium complexes of HN_4bipy (compounds **1** and **2**; see the synthesis below) are performed at the INE-Beamline for actinide research at the ANKA synchrotron facility in Karlsruhe.[33] Samples are measured as powders mounted between polycarbonate tape. Spectra are recorded in transmission and the energy scales calibrated against the first inflection point in the Fe K-edge XANES of a Fe foil, defined as 7.112 eV. Data processing is performed using the Athena code of the *Demeter* package,[34] version 0.9.13. Four scans of **1** and five scans of **2** are averaged, background-subtracted, and normalized.

RESULTS AND DISCUSSION

Synthesis of HN_4bipy and Its Samarium Complexes. HN_4bipy was synthesized by a literature procedure[31] by the treatment of 6-cyano-2,2′-bipyridine with sodium azide and ammonium chloride in DMF at 130 °C for 3 days (Scheme 3). HN_4bipy was precipitated by the addition of an excess 0.1 N HCl solution.

Scheme 3. Synthesis of the HN_4bipy Ligand[30,31,35]

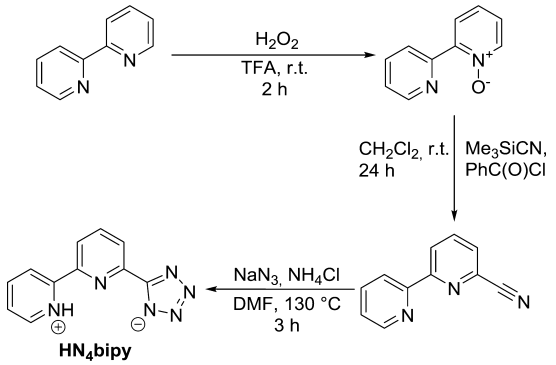

Single crystals of HN_4bipy were obtained from a supersaturated solution in isopropyl alcohol. The solid-state structure of HN_4bipy was established by single-crystal X-ray diffraction (XRD). HN_4bipy crystallizes in the monoclinic space group $P2_1/c$ containing 4 molecules of HN_4bipy and 12 molecules of H_2O in the unit cell (Supporting Information, Figure S1). In the solid state, HN_4bipy is a zwitterionic molecule with a protonated pyridine ring and a deprotonated tetrazolide. The nitrogen atoms N3, N4, and N5, as well as the pyridinium cation, form hydrogen bonds to H_2O molecules. In the tetrazolide anion, the N−N distances lie between 1.328(3) and 1.347(2) Å and the C−N distances are 1.339(3) Å (C11−N3) and 1.334(3) Å (C11−N6), indicating a delocalized anionic structure. The C−N distances in the protonated pyridine ring [1.349(3) Å (C6−N2) and 1.347(3) Å (C10−N2)] are only slightly elongated in comparison with the neutral pyridine ring (1.336 Å) and are in the expected range.[36] More characteristic for pyrdinium cations is the C−N−C angle [C6−N2−C10: 123.7(2)°], which is about 6° larger than that in neutral pyridine rings [C1−N1−C5: 117.9(2)°].[36]

The coordination compound $[Sm(N_4bipy)_2(OH)(H_2O)_2]$ (**1**) was obtained by refluxing 3 equiv. of HN_4bipy with samarium(III) nitrate in isopropyl alcohol. After workup, subsequent crystallization led after 2 weeks to single crystals of **1** (Scheme 4). Complex **1** was characterized by standard analytical and spectroscopic techniques. In comparison with the free HN_4bipy ligand, the signals in ^{1}H and $^{13}C\{^1H\}$ NMR spectra of **1** are broadened because of the paramagnetic moment of the samarium atom. In the $^{13}C\{^1H\}$ NMR spectrum, only 10 of the expected 11 signals were detected. In the IR spectrum, a broad band between ν 3550 and 3000 cm^{-1} for the hydroxyl and water stretch modes is observed. The typical C=N stretch mode of the tetrazolide ion appears at ν 1662 cm^{-1}, which is in agreement with the literature.[37−42]

Compound **1** crystallizes in the monoclinic space group $P2/n$ with two molecules of **1** and seven molecules of H_2O in the

dx.doi.org/10.1021/ic5007549 | Inorg. Chem. 2014, 53, 8949−8958

Scheme 4. Synthesis of 1

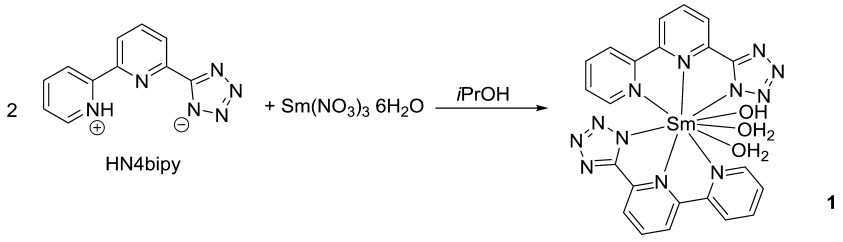

unit cell (Figure 1) and represents the first reported structurally characterized N_4bipy^- complex. The samarium atom is

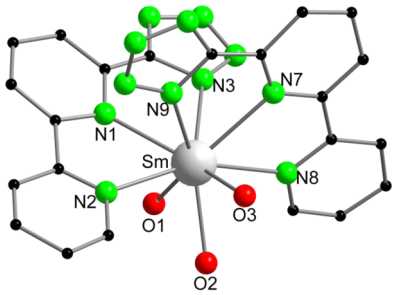

Figure 1. Solid-state structure of **1**. Hydrogen atoms are omitted for clarity.

coordinated by two N_4bipy^- anions, a hydroxide anion, and two H_2O molecules. In contrast to the C5-BPP[14] and dmpbipy[23] ligand complexes, the central atom in **1** is coordinated by two ligands. The hydrogen atoms at the heteroatoms could not be localized in the difference Fourier map. The structural model of **1** is of poor quality so the distances and angles are not discussed. We cannot assign the hydrogen atoms from single-crystal XRD data. Because tetrazoles are very acidic,[43] we consider the ligand to be deprotonated. The pK_a value of HN_4bipy was determined using UV/vis spectroscopy by recording spectra at different conditional pH values and subsequent peak deconvolution with the absorption spectra of the protonated and deprotonated ligands (Supporting Information, Figure S7). Protonation of the ligand occurs at conditional pH values below 3.4, and a pK_a value of 2.2 ± 0.1 is determined.

Complex **1** was also characterized by ESI-MS from a DMF solution (Supporting Information, Figure S2). In the positive-ion spectrum, the base peak at m/z 689.12 amu was assigned to $[Sm(N_4bipy)_2(H_2O)(dmf)]^+$ by spectrum simulation with the software *mMass*.[44,45] The signal at m/z 596.55 amu belongs to the solvent-free dimeric species $[Sm_2(N_4bipy)_4]^{2+}$ (Supporting Information, Figure S3). Between these signals, three signals appear that belong to different solvated $[Sm(N_4bipy)_2]$ species (616.07 amu, $[Sm(N_4bipy)_2(H_2O)]^+$; 634.09 amu, $([Sm(N_4bipy)_2(H_2O)_2]^+$; 671.11 amu, $([Sm(N_4bipy)_2(dmf)]^+)$; Supporting Information, Figure S4).

In the negative-ion spectrum, the deprotonated ligand and its decomposition products at m/z 222.98 ($[N_4bipy]^-$), 194.98 ($[N_4bipy - N_2]^-$), and 166.99 amu ($[N_4bipy - 2N_2]^-$) are observed. The major signal at m/z 668.07 amu is assigned to $[Sm(N_4bipy)_2(OH_2)(H_2O)_2]^-$ (Supporting Information, Figure S5). A complex with three N_4bipy^- ligands is observed at m/z 857.76 amu ($[Sm(N_4bipy)_3(OH)(H_2O)]^-$; Supporting Information, Figure S5).

When the DMF solution with precipitate obtained from the suspension of HN_4bipy and samarium(III) nitrate in isopropyl alcohol is allowed to stand in DMF for about 12 weeks, $[Sm(N_4bipy)_2(HCOO)(H_2O)_2]$ (**2**) forms. Although we reproduced compound **2** once, the long reaction period indicates that a general reproduction of **2** might be difficult. The formate anion is formed by decomposition of DMF to formic acid and dimethylamine.[46] Complex **2** was characterized by standard analytical/spectroscopic techniques. In its ^1H NMR spectrum, broad peaks are observed because of the paramagnetism of the samarium ion. The signal of the formate proton overlaps with the pyridine signals at 8.32 ppm. In the $^{13}C\{^1H\}$ NMR spectrum, no signals could be detected because of the poor solubility of **2** in dimethyl sulfoxide (DMSO). The IR spectrum exhibits the C═N stretch mode of the tetrazolide at ν 1665 cm^{-1}.[37−42] The C−H stretch mode of the formate anion is observed at ν 2925 cm^{-1}. The COO stretch mode, which is expected at ca. 1570 cm^{-1},[47] overlaps with two tetrazolide bands at 1586 and 1568 cm^{-1} and is not observed.

The solid-state structure of **2** was established by single-crystal XRD (Figure 2). It crystallizes in the triclinic space group $P\bar{1}$ with two molecules of **2** and four molecules of DMF in the unit cell. The hydrogen atoms at O3 and O4 were freely refined. The samarium atom has a 9-fold coordination built by two or three dentate N_4bipy^- ligands, one monocoordinating formate anion, and two H_2O molecules.

The formate group coordinates in a monodentate fashion to the samarium atom [Sm−O1: 2.411(2) Å], with a carboxylic oxygen atom forming a hydrogen bond to one of the coordinating H_2O molecules. The distances of the samarium atom to the oxygen atoms of the H_2O molecules are 2.420(2) Å (Sm−O3) and 2.469(2) Å (Sm−O4). The bite angles of the N_4bipy^- ligands are N1−Sm−N2 62.00(6)°, N1−Sm−N3 63.69(7)°, and N2−Sm−N3 125.54°, as well as N7−Sm−N8 61.71(6)°, N7−Sm−N9 63.97(6)°, and N8−Sm−N9 125.60(6)°. In contrast to $[Sm(dmpbipy)(NO_3)_3(dmso)]$,[23] the Sm−N distances of the outer six-membered pyridine ring [Sm−N2 2.591(2) Å; Sm−N8 2.588(2) Å] differ significantly from the Sm−N distances to the five-membered tetrazolate ring [Sm−N3 2.544(2) Å; Sm−N9 2.533(2) Å]. The distance between the samarium ion and the inner pyridine ring is significantly longer [Sm−N1 2.636(2) Å; Sm−N7 2.639(2) Å] and also slightly elongated compared to that for $[Sm(dmpbipy)(NO_3)_3(dmso)]$.[23]

Complex **2** was also characterized by ESI-MS (Supporting Information, Figure S6). In the positive-ion ESI-MS spectrum, two sets of signals were observed. The signal at m/z 744.18 amu can be assigned to $[Sm(N_4bipy)_2(dmf)_2]^+$ (Supporting Information, Figure S6b), which overlaps with a 3-fold-solvated species, $[Sm(N_4bipy)_2(dmf)(^iPrOH)(H_2O)]$, at m/z 749.19 amu (Supporting Information, Figure S6c). At m/z 822.14 amu, a complex species with three ligands is observed

dx.doi.org/10.1021/ic5007549 | Inorg. Chem. 2014, 53, 8949−8958

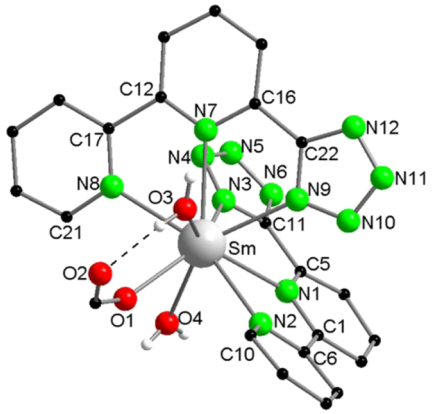

Figure 2. Solid-state structure of **2** omitting carbon-bonded hydrogen atoms. Selected bond lengths [Å] or angles [deg]: C1–N1 1.346(3), C5–N1 1.348(3), C6–N2 1.351(3), C10–N2 1.340(3), C11–N3 1.334(3), C11–N6 1.336(3), C12–N7 1.347(3), C16–N7 1.346(3), C17–N8 1.353(3), C21–N8 1.339(3), C22–N12 1.336(3), C22–N9 1.338(3), C23–O2 1.233(3), C23–O1 1.261(3), N1–Sm 2.636(2), N2–Sm 2.591(2), N3–N4 1.358(3), N3–Sm 2.544(2), N4–N5 1.314(3), N5–N6 1.352(3), N7–Sm 2.639(2), N8–Sm 2.588(2), N9–N10 1.351(3), N9–Sm 2.533(2), N10–N11 1.315(3), N11–N12 1.357(3), O1–Sm 2.411(2), O3–Sm 2.420(2), O4–Sm 2.469(2); N1–C1–C6 116.1(2), N1–C5–C11 114.7(2), N2–C6–C1 116.9(2), N3–C11–N6 112.0(2), N3–C11–C5 121.8(2), N6–C11–C5 126.2(2), N7–C12–C17 116.2(2), N7–C16–C22 115.2(2), N8–C17–C12 116.4(2), N12–C22–N9 111.3(2), N12–C22–C16 126.9(2), N9–C22–C16 121.8(2), C1–N1–C5 118.3(2), C10–N2–C6 118.0(2), C11–N3–N4 104.8(2), N5–N4–N3 108.9(2), N4–N5–N6 109.8(2), C11–N6–N5 104.5(2), C16–N7–C12 118.7(2), C21–N8–C17 118.4(2), C22–N9–N10 105.3(2), N11–N10–N9 109.1(2), N10–N11–N12 109.4(2), C22–N12–N11 104.9(2), N9–Sm–N8 125.60(6), N3–Sm–N2 125.54(6), N3–Sm–N1 63.69(7), N2–Sm–N1 62.00(6), N9–Sm–N7 63.97(6), N8–Sm–N7 61.71(6).

($[Sm(N_4bipy)_2(HN_4bipy)]^+$; Supporting Information, Figure S6d).

XANES Studies. The Sm L3-edge XANES spectra of complexes **1** and **2** are depicted in Figure 3. Inspection of the data reveals that both have nearly the same energy of their white lines (most intense spectral feature; 6720.0 and 6719.5 eV for **1** and **2**, respectively) and the exact same energy of the inflection point (determined as the energy value at the ordinate maximum and zero of the first derivative; 6715.8 eV), indicating that the samples have the same charge, as expected, as well as immeasurable differences in the overall electron donation of coordinating ligands (i.e., similar "chemical shifts"). The two XANES spectra show no significant difference in energy spacing between their white-line position and the next-higher-energy resonance in the XANES spectra (32.3 eV for both **1** and **2**). This energy spacing is expected to vary inversely with the bond distance, so that this observed similarity reflects the small difference in the average of the nine distances in the first oxygen and nitrogen neighbors in the two complexes[48] (complex **1**, 2.55 ± 0.14 Å; complex **2**, 2.54 ± 0.09 Å) determined from XRD analysis. The lower white-line intensity in the XANES spectrum for complex **1** likely is an indication of the larger disorder in the first coordination sphere structure, leading to a widening of the final state d-band associated with the dipole-allowed electron transitions for the Sm L3-edge. This is expressed in the larger variation in the average Sm–O/N distances for this compound (standard deviation of 0.14 Å versus 0.09 Å for **2**). A wider bandwidth would cause a decrease in the probability for the $2p_{5/2}$ electron dipole-allowed transition because generally the transition probability is proportional to the square root of the final state density. Indeed, the d density of states (d-projected DOS) calculated using the XRD data for these two complexes corroborates this interpretation (Supporting Information, Figure S8).

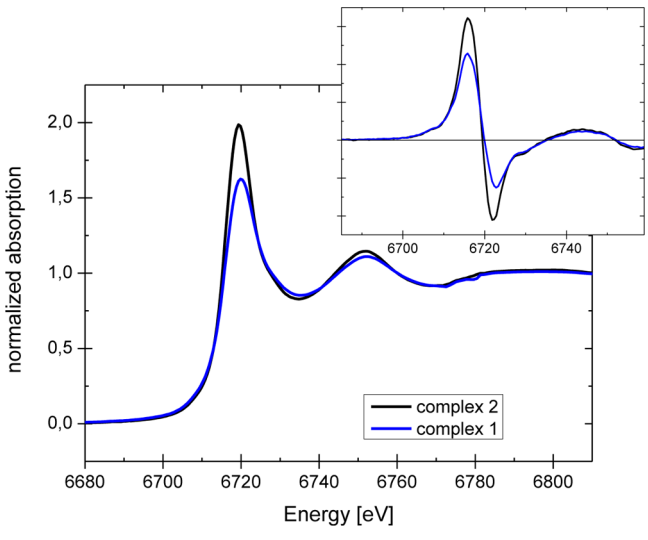

Figure 3. Sm L3-edge XANES spectra and first derivative plots (inset) for complexes **1** and **2**.

TRLFS Studies. Complexation of Cm^{III} and Eu^{III} with HN_4bipy is characterized by TRLFS, which allows us to study and quantify the formation of different complex species in submicromolar concentrations. Furthermore, fluorescence lifetime measurements give access to additional information on the first coordination sphere of the complexes formed. EtOH is chosen as the solvent, in which both the metal ions and the ligand dissolve easily. The initial proton concentrations resulting from the curium(III) and europium(III) stock solutions are 1.5×10^{-4} mol L^{-1} for curium(III) and 4.4×10^{-4} mol L^{-1} for europium(III).

Titrations are performed by the stepwise addition of a HN_4bipy solution to the metal ion solution and subsequent recording of an emission spectrum after each titration step. HN_4bipy is a weak acid (pK_a = 2.2 ± 0.1; see above) and dissociates according to

$$HN_4bipy \rightleftharpoons H^+ + N_4bipy^-$$

Because of the acidity, an increasing ligand concentration results in an increasing proton concentration, which is included in calculation of the species distribution and determination of the stability constants (see below). Regarding the initial proton concentrations, only 2% [in curium(III) complexation studies] and 6% [in europium(III) complexation studies] of the ligand are protonated. Hence, the trivalent metal ions mainly interact with the deprotonated ligand N_4bipy^-. The coordination of both Cm^{III} and Eu^{III} by the N_4bipy^- ligand is confirmed by recording emission spectra at various proton concentrations (Supporting Information, Figures S9 and S10). With increasing proton concentration, protonation of N_4bipy^-, and a subsequent stepwise decomplexation, the formation of less substituted curium(III) and europium(III) complex species is observed (Supporting Information, Figures S9a and S10a).

dx.doi.org/10.1021/ic5007549 | Inorg. Chem. 2014, 53, 8949–8958

The evolution of curium(III) fluorescence spectra resulting from the $^6D'_{7/2} \rightarrow {}^8S'_{7/2}$ transition with increasing concentration of N_4bipy^- is shown in Figure 4a. Without the addition of the ligand, the emission band of the solvated metal ion is observed at λ_{max} = 601.1 nm. This signal is red-shifted in comparison to that for the Cm^{III} aquo ion (with nine H_2O molecules in the first coordination sphere; λ_{max} = 593.7 nm)[49] because of the replacement of H_2O molecules by EtOH molecules in the first coordination sphere. Upon the addition of the ligand solution, two new emission bands are observed. The emission band of the first curium(III) complex species (λ_{max} = 606.5 nm) is hardly distinguishable and only observable at ligand concentrations between 12 and 23 μmol L^{-1}. The emission band of the second species at λ_{max} = 608.9 nm is distinctive at a ligand concentration of >31 μmol L^{-1}.

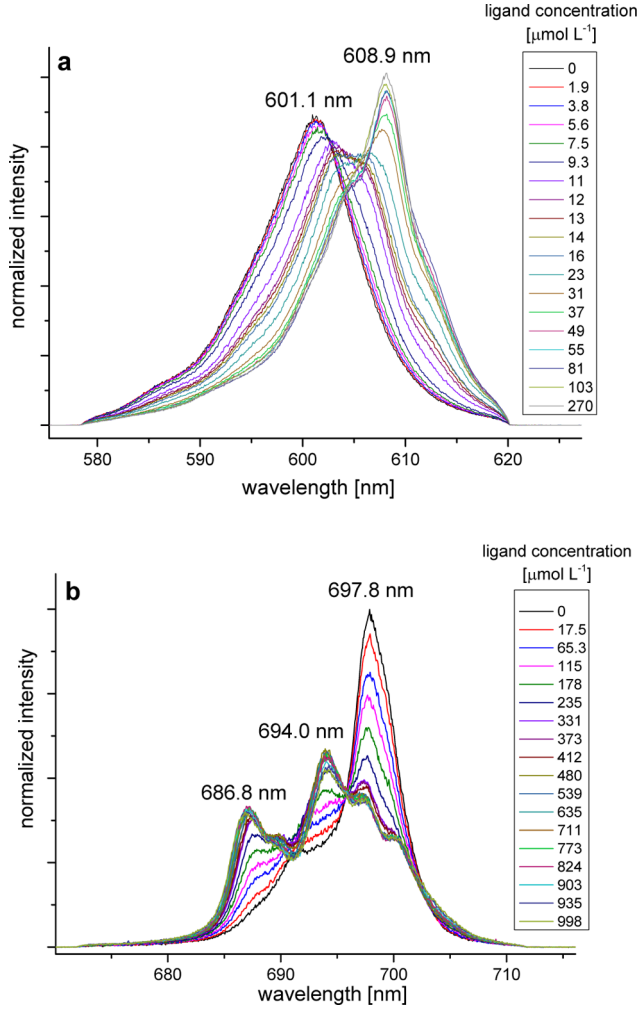

Figure 4. Normalized fluorescence spectra of curium(III) (a) and europium(III) (b) in EtOH (4.4 vol % H_2O) with increasing ligand concentration. $[Cm^{III}]_{ini}$ = 1.0 × 10^{-7} mol L^{-1} and $[Eu^{III}]_{ini}$ = 4.0 × 10^{-5} mol L^{-1}. For a better overview, not all titration steps are shown.

For the effective separation of actinide(III) and lanthanide(III), it is of particular interest to compare the complexation behavior of partitioning relevant nitrogen-donor ligands toward both trivalent actinides and lanthanides. Therefore, investigations are performed with europium(III) under similar conditions. The change of the $^5D_0 \rightarrow {}^7F_4$ emission band of europium(III) at increasing ligand concentration is displayed in Figure 4b. The fluorescence band shows characteristic splitting patterns that are used to distinguish different europium(III) complex species.[50] The $^5D_0 \rightarrow {}^7F_4$ emission band of the solvated metal ion $[Eu(solv.)]^{3+}$ shows a maximum at 697.8 nm and a small shoulder at 691.5 nm. The splitting of the emission band increases upon formation of the Eu^{III}-N_4bipy complex species, and two new species are formed with emission maxima at 687.6, 694.0, and 700.1 nm (first complex species) and at 686.8, 694.1, 697.5, and 700.1 nm (second complex species), respectively.

Spectra were analyzed by peak deconvolution. The relative amounts of the curium(III) and europium(III) complex species are determined using the deconvoluted spectra of the different curium(III) and europium(III) components. To calculate the concentration ratios from these relative species component amounts, fluorescence intensity factors (FI factors) of the different species relative to the solvent species have to be taken into account. For the second curium(III) and europium(III) complex species, higher fluorescence intensities compared to the solvated metal ions are observed (FI[Cm^{III} species 2/$Cm(solv.)^{3+}$] = 3.2 and FI[Eu^{III} species 2/$Eu(solv.)^{3+}$] = 4.5). The FI factors are included in calculation of the species distribution (Figure 5), and from this, stability constants are determined (compare below). The species distributions obtained experimentally are compared with the species

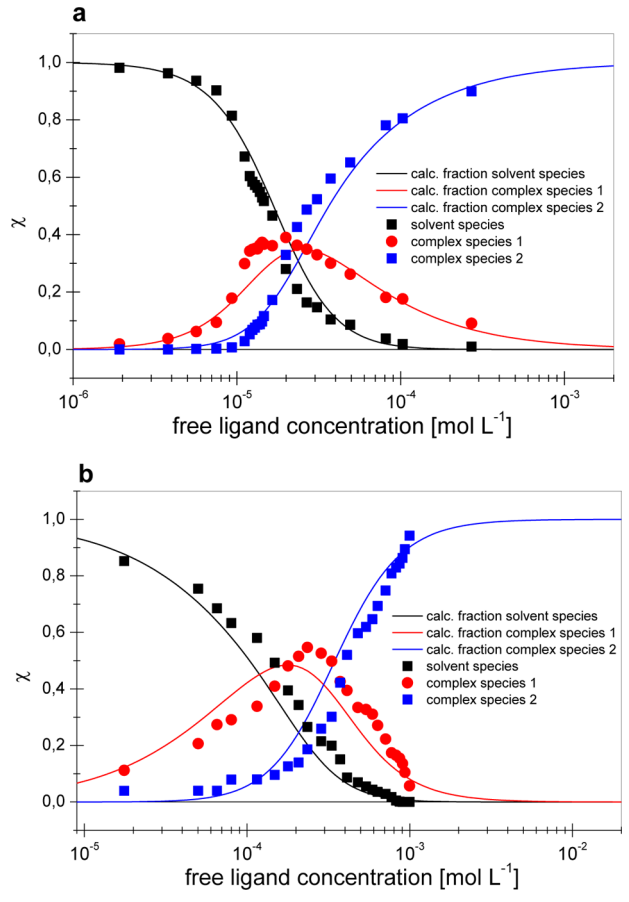

Figure 5. Curium(III) (a) and europium(III) (b) species distribution in EtOH (4.4 vol % H_2O) with increasing free ligand concentration. $[Cm^{III}]_{ini}$ = 1.0 × 10^{-7} mol L^{-1} and $[Eu^{III}]_{ini}$ = 4.0 × 10^{-5} mol L^{-1}. Lines calculated with the conditional stability constants (see Table 1).

dx.doi.org/10.1021/ic5007549 | Inorg. Chem. 2014, 53, 8949−8958

distributions calculated using conditional stability constants (solid lines) (see Table 1).

Table 1. Conditional Stability Constants for the Formation of $[Cm(N_4bipy)_n]^{3-n}$ and $[Eu(N_4bipy)_n]^{3-n}$ (n = 1−3) in EtOH (4.4 vol % H_2O)

metal	log β'_1	log β'_2	log β'_3
curium(III)		9.3 ± 0.2	13.8 ± 0.3
europium(III)	4.0 ± 0.1		11.1 ± 0.2

As shown in Figure 5a, the formation of the first curium(III) complex species is observed at $[N_4bipy]^- = 3.8 \times 10^{-5}$ mol L^{-1}, displaying a maximum relative fraction of 39% at a N_4bipy^- concentration of 2.0×10^{-5} mol L^{-1}. At a N_4bipy^- concentration of 1.2×10^{-5} mol L^{-1}, the second curium(III) complex species starts to form. At N_4bipy^- concentrations of $\geq 2.3 \times 10^{-5}$ mol L^{-1}, this complex is the dominating species in solution. Significantly higher N_4bipy^- concentrations are needed for formation of the europium(III) complex species, which is due to the higher initial europium(III) concentration and lower stability constants (see below).

The first europium(III) complex species is observed at a ligand concentration of $\geq 1.8 \times 10^{-5}$ mol L^{-1}, with a maximum relative fraction of 55% at 2.4×10^{-4} mol L^{-1}. The second europium(III) complex is the dominating complex species at ligand concentrations of $\geq 3.7 \times 10^{-4}$ mol L^{-1}.

Identification of the Complex Species. In order to characterize the complex species formed upon the addition of the N_4bipy^- ligand to solvated curium(III) and europium(III), slope analysis of the speciation results is performed.

The stepwise formation of 1:1, 1:2, and 1:3 curium(III)− and europium(III)−ligand complex species with N_4bipy^- is expressed by the following equilibria:

$$M^{3+} + N_4bipy^- \rightleftharpoons [M(N_4bipy)_1]^{2+}$$

$$[M(N_4bipy)_1]^{2+} + N_4bipy^- \rightleftharpoons [M(N_4bipy)_2]^{+}$$

$$[M(N_4bipy)_2]^{+} + N_4bipy^- \rightleftharpoons [M(N_4bipy)_3]$$

The complex stoichiometry is verified by slope analysis. The logarithm of the complex species ratio is plotted versus the logarithm of the N_4bipy^- concentration according to eq 1.

$$\log\left(\frac{[M(L)_n]}{[M(L)_{n-x}]}\right) = \log K' + x \log[N_4bipy^-] \quad (1)$$

with M = Cm^{III}, Eu^{III}; n = 1−3, x = 1−3, $x \leq n$.

Hence, there is a linear correlation between the logarithm of the concentration ratio $[M(L)_n]/[M(L)_{n-x}]$ and the logarithm of the free ligand concentration with a slope of x. Linear regression of the log−log plots of the concentration ratios from species distribution data and free ligand concentration for the Cm^{III}-N_4bipy complex species gives slopes of 2.0 ± 0.1 for [species 1]/$[Cm(solv.)]^{3+}$ and of 1.1 ± 0.1 for [species 2]/[species 1]. Consequently, the species are identified as a 1:2 $[Cm(N_4bipy)_2]^+$ complex (species 1) and a 1:3 $[Cm(N_4bipy)_3]$ complex (species 2).

For the europium(III) complex species, the following slopes are determined: [species 1]/$[Eu(solv.)]^{3+}$ = 1.0 ± 0.2, [species 2]/[species 1] = 1.9 ± 0.1, and [species 2]/$[Eu(solv.)]^{3+}$ = 3.0 ± 0.1. This indicates that the addition of one ligand to the solvated Eu^{III} metal ion forms a 1:1 $[Eu(N_4bipy)_1]^{2+}$ complex (species 1), and subsequent complexation of two additional ligand molecules forms the 1:3 Eu^{III}-N_4bipy complex (species 2). The formation of a 1:1 metal ion−N_4bipy complex species is observed for Eu^{III} but not for Cm^{III}. To our knowledge, this is the first observation of two different intermediate species (1:1 for Eu^{III} versus 1:2 for Cm^{III}) before formation of the 1:3 metal ion−ligand complex with BTP-type nitrogen-donor ligands.

Depending on the nitrogen-donor ligand and the solvent, in many cases two intermediate complex species (the 1:1 and 1:2 complexes) are observed before the fully coordinated 1:3 complex is formed.[21,24,51] For both the curium(III) and europium(III) complexes with ^{n}Pr-BTP in H_2O/methanol (MeOH), only very small amounts of the 1:1 complex species are observed. The formation of significant amounts of the 1:2 Cm^{III}−ligand species and the absence of a 1:1 Cm_{III}-N_4bipy complex, as well as the absence of the 1:2 Eu^{III}−ligand solution species and rather formation of the 1:3 Eu^{III}−ligand complex species from the 1:1 Eu^{III}−ligand complex, are remarkable.

Determination of Thermodynamic Data. The conditional stability constants of the curium(III) and europium(III) complexes in EtOH (4.4 vol % H_2O) are calculated from the species distributions according to the equilibrium (2) and eq 3.

$$\beta'_n = \frac{[[M(N_4bipy)_n]^{3-n}]}{[M^{3+}]\cdot[N_4bipy^-]^n} \quad (2)$$

$$M^{3+} + nN_4bipy^- \rightleftharpoons [[M(N_4bipy)_n]^{3-n}] \quad (3)$$

with M = Cm^{III}, Eu^{III}; n = 1−3.

According to eq 3, stability constants of log β'_2 = 9.3 ± 0.2 and log β'_3 = 13.8 ± 0.3 are determined for curium(III). The log β'_3 value is 1 and 5−6 orders of magnitude lower in comparison to values for 1:3 curium(III) complex species with other highly effective extracting agents like C5-BPP[21] and ^{n}Pr-BTP[13] measured in comparable solvent mixtures.[52]

For the europium(III) complex species, stability constants of log β'_1 = 4.0 ± 0.1 and log β'_3 = 11.1 ± 0.2 are derived. Stability constants for formation of the curium(III) and europium(III) complex species are summarized in Table 1.

Hence, under the applied conditions, the log β'_3 value for the formation of $[Eu(N_4bipy)_3]$ is 2.7 orders of magnitude lower than the stability constant for the formation of $[Cm(N_4bipy)_3]$. This results in a theoretical separation factor $SF_{Cm^{III}/Eu^{III}} = \beta'_{3,Cm^{III}}/\beta'_{3,Eu^{III}} \approx 500$, which is in the same order of magnitude as the values determined for ^{n}Pr-BTP ($SF_{Cm^{III}/Eu^{III}} = 320$)[8,13] or C5-BPP ($SF_{Cm^{III}/Eu^{III}} \approx 100$).[21]

Influence of a Lipophilic Anion Source. For many BTP-type ligands, a lipophilic anion source such as 2-bromodecanoic acid is required for extraction of the trivalent actinides and lanthanides into an organic solvent.[8,12,20−22] The lipophilic anion source helps to extract the complexes formed between the actinide(III) and tridentate nitrogen-donor ligand from the aqueous phase into the organic phase. The extraction mechanism follows an ion-exchange mechanism:

$$M^{3+}_{aq} + 3HA_{org} + nL_{org} \rightleftharpoons [MA_3(L)_n]_{org} + 3H^+_{aq}$$

with HA = 2-bromodecanoic acid and L = nitrogen-donor ligand.

Because curium(III) emission bands show a distinct shift upon subtle changes in the first coordination sphere of the metal ion, curium(III) is used for complexation studies in the presence of 0.1 mol L^{-1} 2-bromodecanoic acid. In the presence of 0.1 mol L^{-1} 2-bromodecanoic acid and without added ligand,

dx.doi.org/10.1021/ic5007549 | Inorg. Chem. 2014, 53, 8949−8958

the emission band of the solvated metal ion $[Cm(solv.)]^{3+}$ is observed at λ_{max} = 601.5 nm. The small bathochromic (0.4 nm) shift of the solvated curium(III) in comparison to the solvated curium(III) in the absence of 2-bromodecanoic acid is explained by a partial replacement of solvent molecules in the first coordination sphere by 2-bromodecanoate.

Upon increasing ligand concentration (Figure 6), an emission band is observed at λ_{max} = 608.9 nm. Because of a weak interaction of Cm^{III} with 2-bromodecanoic acid, the complex species forms at slightly higher ligand concentration compared to the titration experiment performed in the absence of the lipophilic anion. Analysis of the spectra in a manner analogous to treatment of the data without 2-bromodecanoic acid described above confirms the existence of an intermediate species in this case too. In the presence of 2-bromodecanoic acid, a slightly lower fluorescence intensity for complex species 2 compared to the solvated metal ion is observed: FI[complex species 2] = 1.6. The speciation diagram is shown in Figure 6b. The intermediate species is formed at ligand concentrations of $>5.7 \times 10^{-6}$ mol L^{-1} and shows a maximum fraction of 53% at a ligand concentration of 5.3×10^{-5} mol L^{-1}. For ligand concentrations of $>8.6 \times 10^{-5}$ mol L^{-1}, the second complex species at λ_{max} = 608.9 nm becomes the dominating species.

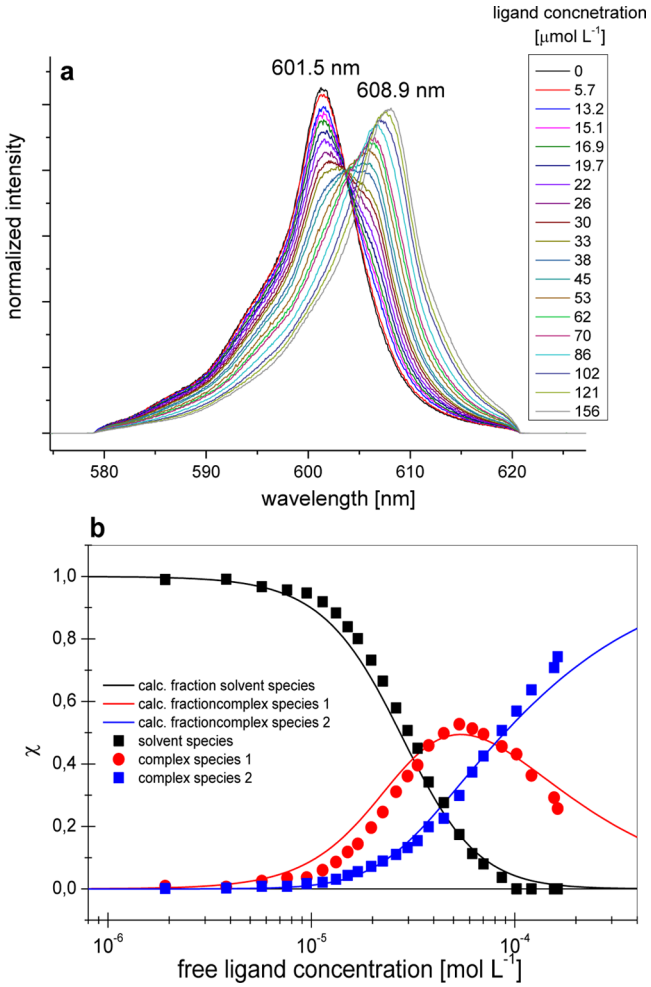

Figure 6. (a) Normalized fluorescence spectra of curium(III) in EtOH/0.1 mol L^{-1} 2-bromodecanoic acid with increasing free ligand concentration. For a better overview, not all titration steps are shown. (b) Speciation in EtOH/0.1 mol L^{-1} 2-bromodecanoic acid with increasing ligand concentration. $[Cm^{III}]_{ini} = 1.0 \times 10^{-7}$ mol L^{-1}. Lines calculated with the conditional stability constants given in Table 2

Linear regression of the experimental data according to eq 1 yields slopes of 2.2 ± 0.1 for the intermediate species and 3.0 ± 0.1 for the final complex species, indicating the formation of $[Cm(N_4bipy)_2]^+$ and $[Cm(N_4bipy)_3]$ complex species, in agreement with the results of the titration experiment performed in the absence of 2-bromodecanoic acid. The following conditional stability constants are determined: log β'_2 = 9.0 ± 0.1 and log β'_3 = 13.1 ± 0.2 (see Table 2).

Table 2. Conditional Stability Constants for the Formation of $[Cm(N_4bipy)_n]^{3-n}$ (n = 2, 3) in the Presence and Absence of 0.1 mol L^{-1} 2-Bromodecanoic acid

solvent	log β'_2	log β'_3
EtOH	9.3 ± 0.2	13.8 ± 0.3
EtOH, 0.1 M $C_{10}H_{19}BrO_2$	9.0 ± 0.1	13.1 ± 0.2

It is shown that the fully coordinated 1:3 Cm^{III}-N_4bipy complex species is formed with or without a lipophilic anion. The formation of ternary complexes is not observed. The stability constants are smaller in the presence of 2-bromohexanoic acid than in the absence of 2-bromohexanoic acid (see Table 2). This is explained by a weak competition between the ligand and lipophilic anion as a ligand for curium(III). This is in agreement with the earlier results for 1:3 curium(III) complexes with C5-BPP, where an even more pronounced difference in the stability constants was observed (log $\beta_{3,Cm^{III}}$ = 14.8 ± 0.4 in MeOH;[21] log $\beta_{3,Eu^{III}}$ = 13.3 ± 0.4 in MeOH/0.1 M 2-bromodecanoic acid).[20]

Fluorescence Lifetime Studies. Further information on the inner coordination sphere of the $[Cm(N_4bipy)_3]$ and $[Eu(N_4bipy)_3]$ complex species is obtained by determination of the fluorescence lifetimes. For $Cm(N_4bipy)_3$, a fluorescence lifetime of τ = 270 ± 13 µs is determined in EtOH and τ = 271 ± 12 µs in EtOH/0.1 mol L^{-1} 2-bromodecanoic acid (Supporting Information, Figure S11). Hence, equal fluorescence lifetimes confirm the formation of identical final complex species in the presence and absence of 2-bromodecanoic acid. The observed fluorescence lifetime of the $[Cm(N_4bipy)_3]$ complex is shorter than the fluorescence lifetime of the 1:3 Cm^{III}-^{n}Pr-BTP complexes[13] but longer than, for example, the lifetime values determined for $Cm(^n$Pr-Tetrazine$)_3$ (τ = 164 µs) or Cm(Et-BDP)$_3$ (τ = 144 µs).[24] Moreover, the obtained curium(III) fluorescence lifetime values are significantly shorter than the calculated fluorescence lifetime of 1.3 ms expected for curium(III) with 9-fold coordination, in which all nine coordinating solvent molecules are replaced by three tridentate ligands.[53] The observed shorter fluorescence lifetime originates from a quenching process via intramolecular energy transfer from the metal ion excited state to a low-lying triplet state of the organic ligand.[54] This effect was also observed for other curium(III) complexes with a variety of aromatic nitrogen-donor ligands.[13,24,51]

For $[Eu(N_4bipy)_3]$, a fluorescence lifetime of 617 ± 48 µs is determined in EtOH and 592 ± 45 µs in EtOH/0.1 mol L^{-1} 2-bromodecanoic acid (Supporting Information, Figure S11). The fluorescence lifetimes of $[Eu(N_4bipy)_3]$ in both solvents are significantly shorter than the lifetime of other BTP-type ligands in H_2O[51] or H_2O/MeOH,[13] indicating a significantly stronger fluorescence quenching by the HN_4bipy ligand in contrast to nitrogen-donor ligands like ^{n}Pr-BTP or aq-BTP.

dx.doi.org/10.1021/ic5007549 | Inorg. Chem. 2014, 53, 8949−8958

The europium(III) lifetime values differ more in comparison to the fluorescence lifetimes of $[Cm(N_4bipy)_3]$ in the presence and absence of 2-bromodecanoic acid. However, within the error range, europium(III) fluorescence lifetime data obtained in both systems are comparable, proving that the same final complex species are formed.

Liquid–Liquid Extraction. Due to the significant difference in the conditional stability constants log $\beta'_{3,Cm^{III}}$ and log $\beta'_{3,Eu^{III}}$, high separation factors for the separation of trivalent lanthanides and actinides ($SF_{Am^{III}/Eu^{III}} = D_{Am^{III}}/D_{Eu^{III}}$) are expected in biphasic liquid–liquid extraction. To study the extraction performance of this tetrazolylbipyridine ligand class, an initial extraction test was performed. Unfortunately, because of the low solubility of HN_4bipy in nonpolar solvents like 1-octanol and precipitation of the ligand upon the addition of the organic ligand solution, no extraction of americium(III) and europium(III) into the organic phase is observed. Because of the excellent complexation properties and the high selectivity for actinide(III) over lanthanide(III), we now endeavor to synthesize a HN_4bipy-type ligand containing lipophilic *tert*-butyl moieties in the para position to one of the bipyridine nitrogen atoms, in order to improve the solubility of the ligand in nonpolar solvents.

CONCLUSION

In this study, the coordination properties of HN_4bipy are examined and compared to the results for similar but systematically structurally varied ligands to understand the influence of the ligand geometry on the coordination behavior. In contrast to earlier studies with dmpbipy and C5-BPP, two N_4bipy^- ligand molecules coordinate the samarium center in the solid-state compound. Two different solid 1:2 complexes, $[Sm(N_4bipy)_2(OH)(H_2O)_2]$ (**1**) and $[Sm(N_4bipy)_2(HCOO)(H_2O)_2]$ (**2**), have been obtained as model complexes and were fully characterized. These are the first structurally characterized complexes bearing the N_4bipy^- ligand.

TRLFS titration experiments with curium(III) have shown that two different complexes, a 1:2 and a 1:3 Cm^{III}-N_4bipy complex, form in solution, whereas in the case of europium(III), the formation of a 1:1 and a 1:3 Eu^{III}-N_4bipy complex is observed. Conditional stability constants are determined for the fully coordinated complex species: log $\beta_3[Cm(N_4bipy)_3] = 13.8 \pm 0.3$ and log $\beta_3[Eu(N_4bipy)_3] = 11.1 \pm 0.2$. Thus, N_4bipy^- forms more stable 1:3 complexes with Cm^{III} than with Eu^{III}, associated with a theoretical separation factor $SF_{Cm^{III}/Eu^{III}} \approx 500$. This pronounced selectivity has an order of magnitude comparable to that of ^{n}Pr-BTP complexes, which demonstrates the extraordinary complexation behavior of HN_4bipy. The complexation of Cm^{III} with HN_4bipy in the presence of the lipophilic anion source 2-bromodecanoic acid shows that 1:2 and 1:3 complex species also form in this case; the formation of ternary complexes is excluded. The determined conditional stability constant of the 1:3 curium(III) complex species (log $\beta_3 = 13.1 \pm 0.2$) in the presence of 2-bromohexanoic acid is 0.7 orders of magnitude lower than that in its absence, which is attributed to a weak competition between the HN_4bipy ligand and 2-bromodecanoic acid.

Addressing our aim of understanding the influence of the ligand geometry on coordination behavior, we compare these results with previous results for BTPs.[55] Our studies of various nitrogen-donor ligand systems show a trend toward the enhanced stability of the actinide complexes over their lanthanide counterparts for complexes with a large number of heterocycle nitrogen atoms. The 1:3 complex in this case has nine coordinating nitrogen atoms, as does the 1:3 BTP complex. Because of the low solubility of HN_4bipy in nonpolar solvents such as 1-octanol or kerosene, no extraction of $^{241}Am^{III}$ or $^{152}Eu^{III}$ from nitric acid into the organic phase is observed. Therefore, the synthesis of a more lipophilic HN_4bipy-type ligand and associated characterization is now in progress.

ASSOCIATED CONTENT

Supporting Information

Figures S1–S11 and X-ray crystallographic files in CIF format for the structure determinations of HN_4bipy, **1**, and **2**. This material is available free of charge via the Internet at http://pubs.acs.org.

AUTHOR INFORMATION

Corresponding Authors

*E-mail: petra.panak@kit.edu.
*E-mail: roesky@kit.edu.

Notes

The authors declare no competing financial interest.

ACKNOWLEDGMENTS

This work is supported by the German Federal Ministry of Education and Research (BMBF) under Contracts 02NUK020A, 02NUK020B, 02NUK012D, 02NUK012A, 02NUK012B, and 02NUK020D. Dr. Olaf Fuhr is acknowledged for recording ESI-MS spectra.

REFERENCES

(1) *IEA—Key World Energy Statistics 2012*; International Energy Agency (IEA): Paris, France, 2012.
(2) Gompper, K.; Geist, A.; Geckeis, H. *Nachr. Chem.* **2010**, *58*, 1015.
(3) Ekberg, C.; Fermvik, A.; Retegan, T.; Skarnemark, G.; Foreman, M. R. S.; Hudson, M. J.; Englund, S.; Nilsson, M. *Radiochim. Acta* **2008**, *96*, 225.
(4) Kolarik, Z. *Chem. Rev.* **2008**, *108*, 4208.
(5) Lewis, F. W.; Harwood, L. M.; Hudson, M. J.; Drew, M. G. B.; Modolo, G.; Sypula, M.; Desreux, J. F.; Bouslimani, N.; Vidick, G. *Dalton Trans.* **2010**, *39*, 5172.
(6) Madic, C.; Boullis, B.; Baron, P.; Testard, F.; Hudson, M. J.; Liljenzin, J. O.; Christiansen, B.; Ferrando, M.; Facchini, A.; Geist, A.; Modolo, G.; Espartero, A. G.; De Mendoza, J. *J. Alloys Compd.* **2007**, *444–445*, 23.
(7) Musikas, C.; Vitorge, P.; Pattee, D. *Proc. Int. Solvent Extraction Conf. (ISEC '83)* **1983**, 6.
(8) Panak, P. J.; Geist, A. *Chem. Rev.* **2013**, *113*, 1199.
(9) Lewis, F. W.; Hudson, M. J.; Harwood, L. M. *Synlett* **2011**, 2609.
(10) Hudson, M. J.; Harwood, L. M.; Laventine, D. M.; Lewis, F. W. *Inorg. Chem.* **2012**, *52*, 3414.
(11) Kolarik, Z.; Müllich, U.; Gassner, F. *Solvent Extr. Ion Exch.* **1999**, *17*, 1155.
(12) Kolarik, Z.; Müllich, U.; Gassner, F. *Solvent Extr. Ion Exch.* **1999**, *17*, 23.
(13) Trumm, S.; Panak, P. J.; Geist, A.; Fanghänel, T. *Eur. J. Inorg. Chem.* **2010**, 3022.
(14) Drew, M. G. B.; Guillaneux, D.; Hudson, M. J.; Iveson, P. B.; Russell, M. L.; Madic, C. *Inorg. Chem. Commun.* **2001**, *4*, 12.
(15) Berthet, J.-C.; Miquel, Y.; Iveson, P. B.; Nierlich, M.; Thuery, P.; Madic, C.; Ephritikhine, M. *J. Chem. Soc., Dalton Trans.* **2002**, 3265.
(16) Colette, S.; Amekraz, B.; Madic, C.; Berthon, L.; Cote, G.; Moulin, C. *Inorg. Chem.* **2004**, *43*, 6745.
(17) Iveson, P. B.; Riviere, C.; Guillaneux, D.; Nierlich, M.; Thuery, P.; Ephritikhine, M.; Madic, C. *Chem. Commun.* **2001**, 1512.

(18) Denecke, M. A.; Panak, P. J.; Burdet, F.; Weigl, M.; Geist, A.; Klenze, R.; Mazzanti, M.; Gompper, K. *C. R. Chim.* **2007**, *10*, 872.
(19) Denecke, M. A.; Rossberg, A.; Panak, P. J.; Weigl, M.; Schimmelpfennig, B.; Geist, A. *Inorg. Chem.* **2005**, *44*, 8418.
(20) Bremer, A.; Geist, A.; Panak, P. J. *Radiochim. Acta* **2013**, *101*, 285.
(21) Bremer, A.; Ruff, C. M.; Girnt, D.; Müllich, U.; Rothe, J.; Roesky, P. W.; Panak, P. J.; Karpov, A.; Müller, T. J. J.; Denecke, M. A.; Geist, A. *Inorg. Chem.* **2012**, *51*, 5199.
(22) Bremer, A.; Geist, A.; Panak, P. J. *Dalton Trans.* **2012**, *41*, 7582.
(23) Girnt, D.; Roesky, P. W.; Geist, A.; Ruff, C. M.; Panak, P. J.; Denecke, M. A. *Inorg. Chem.* **2010**, *49*, 9627.
(24) Beele, B. B.; Rüdiger, E.; Schwörer, F.; Müllich, U.; Geist, A.; Panak, P. J. *Dalton Trans.* **2013**, 12139.
(25) Steppert, M.; Walther, C.; Geist, A.; Fanghanel, T. *New J. Chem.* **2009**, *33*, 2437.
(26) Halcrow, M. A. *Coord. Chem. Rev.* **2005**, *249*, 2880.
(27) Hudson, M. J.; Boucher, C. E.; Braekers, D.; Desreux, J. F.; Drew, M. G. B.; Foreman, M. R. S. J.; Harwood, L. M.; Hill, C.; Madic, C.; Marken, F.; Youngs, T. G. A. *New J. Chem.* **2006**, *30*, 1171.
(28) Trumm, S.; Geist, A.; Panak, P. J.; Fanghänel, T. *Solvent Extr. Ion Exch.* **2011**, *29*, 213.
(29) Trumm, S.; Wipff, G.; Geist, A.; Panak, P. J.; Fanghänel, T. *Radiochim. Acta* **2011**, *99*, 13.
(30) Heirtzler, F. R. *Synlett* **1999**, 1203.
(31) Song, Y.-H.; Chiu, Y.-C.; Chi, Y.; Chou, P.-T.; Cheng, Y.-M.; Lin, C.-W.; Lee, G.-H.; Carty, A. J. *Organometallics* **2007**, *27*, 80.
(32) Sheldrick, G. *Acta Crystallogr., Sect. A* **2008**, *64*, 112.
(33) Rothe, J.; Butorin, S.; Dardenne, K.; Denecke, M. A.; Kienzler, B.; Löble, M.; Metz, V.; Seibert, A.; Steppert, M.; Vitova, T.; Walther, C.; Geckeis, H. *Rev. Sci. Instrum.* **2012**, *83*.
(34) Ravel, B.; Newville, M. *J. Synchrotron Radiat.* **2005**, *12*, 537.
(35) Demnitz, F. W. J.; D'Heni, M. B. *Org. Prep. Proced. Int.* **1998**, *30*, 467.
(36) Bowen, R. J.; Fernandes, M. A.; Gitari, P. W.; Layh, M. *Acta Crystallogr., Sect. C* **2004**, *60*, o113.
(37) Lasri, J.; Fernández Rodríguez, M. J.; Guedes da Silva, M. F. C.; Smoleński, P.; Kopylovich, M. N.; Fraústo da Silva, J. J. R.; Pombeiro, A. J. L. *J. Organomet. Chem.* **2011**, *696*, 3513.
(38) Lin, P.; Clegg, W.; Harrington, R. W.; Henderson, R. A. *Dalton Trans.* **2005**, *0*, 2388.
(39) Mukhopadhyay, S.; Lasri, J.; Guedes da Silva, M. F. C.; Januário Charmier, M. A.; Pombeiro, A. J. L. *Polyhedron* **2008**, *27*, 2883.
(40) Mukhopadhyay, S.; Lasri, J.; Januario Charmier, M. A.; Guedes da Silva, M. F. C.; Pombeiro, A. J. L. *Dalton Trans.* **2007**, *0*, 5297.
(41) Mukhopadhyay, S.; Mukhopadhyay, B. G.; Guedes da Silva, M. F. C.; Lasri, J.; Charmier, M. A. l. J. r.; Pombeiro, A. J. L. *Inorg. Chem.* **2008**, *47*, 11334.
(42) Smolenski, P.; Mukhopadhyay, S.; Guedes da Silva, M. F. C.; Charmier, M. A. J.; Pombeiro, A. J. L. *Dalton Trans.* **2008**, *0*, 6546.
(43) Lieber, E.; Patinkin, S. H.; Tao, H. H. *J. Am. Chem. Soc.* **1951**, *73*, 1792.
(44) Strohalm, M.; Hassman, M.; Košata, B.; Kodíček, M. *Rapid Commun. Mass Spectrom.* **2008**, *22*, 905.
(45) Strohalm, M.; Kavan, D.; Novák, P.; Volný, M.; Havlíček, V. r. *Anal. Chem.* **2010**, *82*, 4648.
(46) Juillard, J. *Pure Appl. Chem.* **1977**, *49*, 885.
(47) Ito, K.; Bernstein, H. J. *Can. J. Chem.* **1956**, *34*, 170.
(48) The difference between the white line and the first EXAFS resonance is proportional to $1/R^2$.
(49) Klenze, R.; Kim, J. I.; Wimmer, H. *Radiochim. Acta* **1991**, *52*−*53*, 97.
(50) Wilden, A.; Modolo, G.; Lange, S.; Sadowski, F.; Beele, B. B.; Skerencak-Frech, A.; Panak, P. J.; Iqbal, M.; Verboom, W.; Geist, A.; Bosbach, D. *Solvent Extr. Ion Exch.* **2014**, *32*, 119.
(51) Ruff, C. M.; Müllich, U.; Geist, A.; Panak, P. J. *Dalton Trans.* **2012**, *41*, 14594.
(52) Bremer, A. Doctoral Dissertation, University of Heidelberg, Heidelberg, Germany, 2014.
(53) Beitz, J. V. *Handbook on the Physics and Chemistry of Rare Earths*; Elsevier: Amsterdam, The Netherlands, 1994; Vol. *18*.
(54) Panak, P.; Klenze, R.; Kim, J. I.; Wimmer, H. *J. Alloys Compd.* **1995**, *225*, 261.
(55) Banik, N. L.; Denecke, M. A.; Geist, A.; Modolo, G.; Panak, P. J.; Rothe, J. *Inorg. Chem. Commun.* **2013**, *29*, 172.